Beam Scanning UHF RFID Reader Antenna with High Gain and Wide Axial Ratio Beamwidth

Rui Chen[1], Shuai Yang[1], *Member, IEEE*, Ajeck M. Ndifon[1], *Student Member, IEEE*, Ian H. White[2], *Fellow, IEEE*, Richard V. Penty[1], *Senior Member, IEEE* and Michael Crisp[1], *Member, IEEE*

***Abstract*—A novel ultra-high-frequency (UHF) RFID reader antenna is proposed, designed and measured. The proposed antenna is capable of 2-dimensional (2D) beam-scanning from 0° to 360° in the azimuth plane, and 0° to 40° in the zenith plane. The minima of the antenna's axial ratio (AR) follows its gain maxima during beam-scanning, resulting in an equivalent 3 dB AR beamwidth of over 136° for every phi cut. Moreover, the antenna's AR can be easily modified without affecting other parameters. It is shown experimentally that the antenna's 2D beam-scanning ability and the improved AR performance lead to better tag-reading results, improving the percentage of missing tags by up to 21.6% compared to a standard antenna which has a degraded AR and only supports 1D beam-scanning. In addition, the antenna needs no matching network and has a -10 dB return loss bandwidth from 860 MHz to 880 MHz.**

***Index Terms*—Antenna arrays, Phased arrays, Radio-frequency identification, UHF antennas, UHF propagation**

I. Introduction

There are two major problems in a practical passive UHF RFID systems. Firstly, tags are almost always linearly polarised and randomly oriented [1], and thus, a polarisation mismatch between a linear reader antenna and the tag antenna results in a reduced received RF power at the tag's integrated circuit (IC). Secondly, RF signals in the UHF band are susceptible to multipath effects, i.e. the reflected signals from walls or other objects commonly found indoors interfere with the direct line-of-sight (LoS) signal. When these signals are 180°out of phase with each other, destructive interference occurs, causing signal nulls where the power level at the tag is below the tag sensitivity, preventing successful identification. Thus, to effectively eliminate the above two problems, an improved reader antenna should:

- be circularly polarised **(CP)** to minimise the polarisation mismatch
- be able to beam-steer, so that the severity and the likelihood of signal nulls can be reduced by placing less power into reflected paths

The regulations (FCC and ETSI) also permit a higher EIRP if the beamwidth of the antenna is <90°, so beam steering with a narrower beamwidth is desirable to maximise the coverage from a single antenna.

Manuscript received January 29, 2020; accepted xxxxxx, 2020. Date of publication xxxxxx, 2020; date of current version April 27, 2020. This work was supported by EPSRC EP /S-19405/1 Channel Optimised Distributed Passive Sensor Networks. (Corresponding author: Rui Chen (rc714@cam.ac.uk)).

[1]: the authors are with the Electrical Division, Department of Engineering, University of Cambridge, Cambridge, CB3 1PZ, U.K.

[2]: the author is within Claverton Down, University of Bath, BA2 7AY, U.K.

Digital Object Identifier xxxxxxxxxxx

However, practical antennas are not perfectly circularly polarised in every direction. Typically, they have a minimum AR and **an** AR beamwidth which could influence the reading of linearly polarised tags with different orientations. Take the two antennas in Fig. 1 as an example. Both antennas are CP antennas, but their 3 dB AR beamwidths are very different. The reader antenna with a lower AR **and a wider AR beamwidth** is more insensitive to tag orientation and it is therefore expected that their tag-reading performance would also be different.

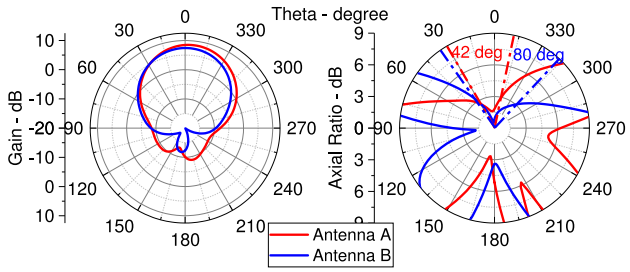

Fig. 1. A comparison of two commercial antennas on beamwidth (left) and axial ratio (right) at $\varphi = 0°$ cut. These antennas are measured in an MVG StarLab antenna characterization chamber [2]

Instead of beam-scanning in a single plane, a 2D beam-scanning as shown in Figs. 9 and 10 gives an additional dimension of freedom to the antenna when battling against the multipath effect. It also enables the antenna to have a wider interrogation coverage. **This paper is focused on the development of an antenna with a combination of good AR, wide AR beamwidth and 2D beam scanning capability.**

TABLE I
A COMPARISON OF THE PROPOSED ANTENNA WITH ANTENNAS IN LITERATURE [3]

	[4]	[5]	[6]	[7]	**This work**
Beam-scanning	1D	1D	1D	2D	2D
3dB AR beamwidth	25°	LP	60°	38°	136° (with scanning)
Matching network requirement	Yes	Yes	No	Yes	No
Gain (dB)	7.1	6.5	10	12.5	10.5

A comparison of this work to antennas reported in the literature is given in Table I. **The proposed antenna** has a close to 0 dB AR around its beam maxima. This AR minima follows the gain maxima during beam-steering, giving a wide equivalent 3 dB AR beamwidth of 136°, in every φ cut; Further, it is capable of steering its beam from 0° to 360°

in azimuth, and 0° to 40° in zenith. In addition, as will be shown **experimentally** in Section IV, the antenna's improved AR and its 2D beam-steering ability **lead to an improved RFID tag detection.**

The rest of this paper is organised as follows: Section II introduces the antenna design, including parameter selection, design and optimisation procedures and full-wave simulation results. Section III presents the measurement results of the manufactured antenna and compares them with the simulation results and those of a conventional off-the-shelf 2-by-2 phased array. Section IV compares the antenna's tag-reading performance in various configurations, and shows the improvements gained from the antenna's enhanced AR and beam-steering ability. Finally, a conclusion is given in section V.

II. Antenna Design and Performance Evaluation

From [8], it is known that a conventional loop antenna with a single feed and a ground plane is linearly polarised in the far field. Using either a vector potential analysis or full-wave simulation, it is revealed that along such a loop, a standing wave **current distribution** with two peaks **is** formed as shown in Fig. 2. The locations of these two peaks are fixed, making it analogous to the current distribution of a bent dipole. The dominant electric field component of the antenna in its far-field is E_y as in shown Fig. 2 [9], and the loop is linearly polarised.

The authors of [10] suggest that circular polarisation can be stimulated by adding a perturbation line (PL) with a certain length to a loop antenna. A detailed mathematical analysis can be found in [10], [11], but in brief, this is due to the reflected current from the PL interacting with the current **at the junction**, leading to a travelling wave current with a uniform amplitude and a linearly-changing phase as shown in Figs. 3 and 4 [9]. This is analogous to physically rotating the loop around its axis once per cycle, hence stimulating a circular polarisation.

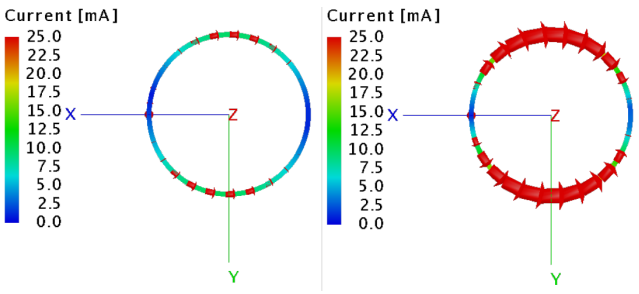

Fig. 2. Current distribution for a conventional 1λ loop antenna with standing-wave-type current. Left: t=0, right: t=T/4 [3]

As introduced in [8] a 1λ loop antenna generates an axial beam. Thus, two extra loops with perimeters at approximately 2λ and 3λ are added in the design. Each of these two loops will produce a conical beam pattern when fed in isolation. When operating the antenna as a whole, beam-steering can be achieved by manipulating the relative phase and amplitude of those three loops.

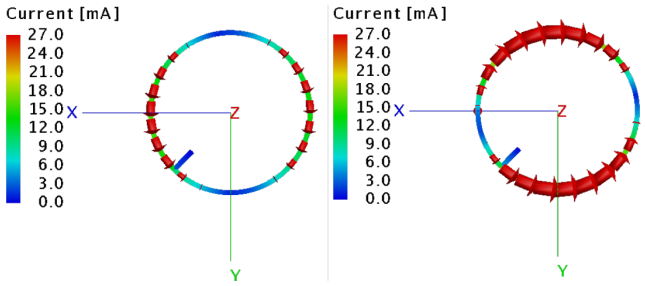

Fig. 3. Current distribution for a 1λ loop antenna with traveling-wave-type current. Left: t=0, right: t=T/4 [3]

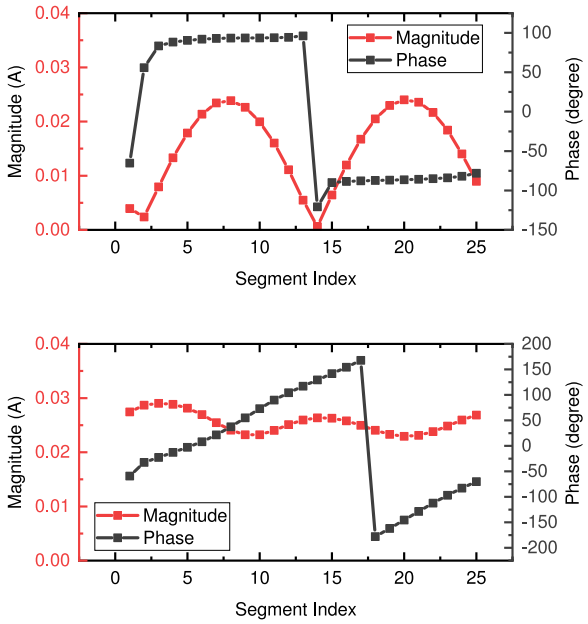

Fig. 4. Amplitude and phase distribution of the current on a 1λ loop antenna. Top: a conventional loop with standing-wave current distribution, bottom: a loop with a perturbation element showing traveling-wave current distribution [9]

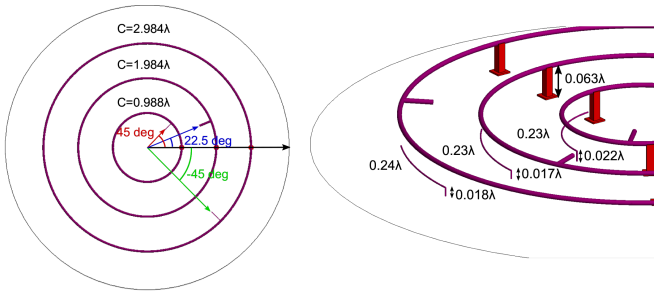

Fig. 5. The top view and side view of the proposed antenna structure [9]

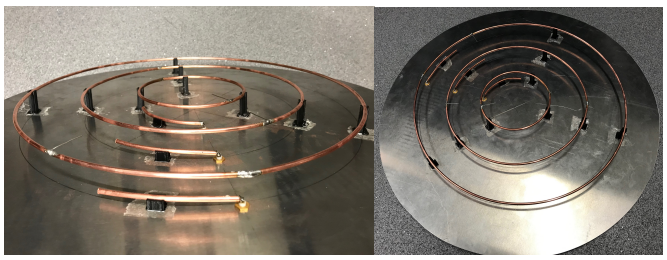

Fig. 6. **The manufactured antenna in different views [9]**

A. Antenna Design and Simulation

The 3D model and the manufactured prototype of the proposed antenna are shown in Figs. 5 [9] and 6 respectively. The radiating layer is at the top of the antenna, which is composed of three concentric loops, each with a PL for the generation of circular polarisation [3], [9]. The position and length of these perturbation lines need to be carefully adjusted as they will affect the antenna's AR performance [3]. **The detailed optimisation process shown in [3] has been adopted here. An example of optimising the isolated inner ring is given in Fig. 7 [9].**

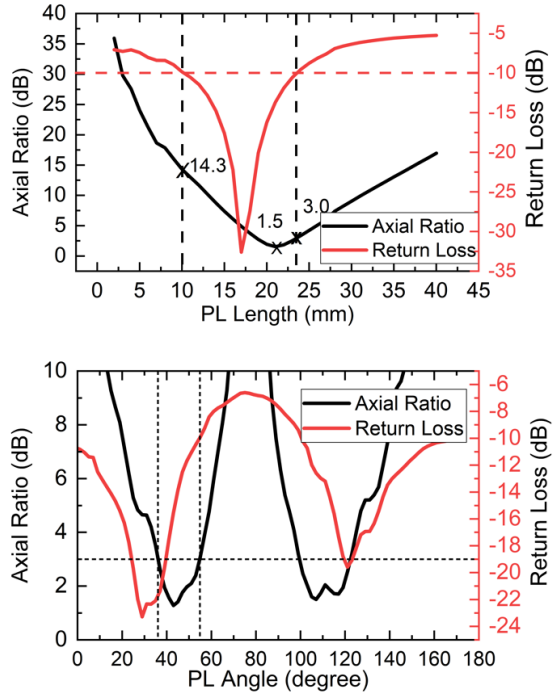

Fig. 7. **Top: The simulated axial ratio (the observation point is set at the gain maxima of the loop at $(\theta, \varphi) = (0, 0)$) and return loss of the first loop against various PL lengths, with a fixed PL position at $45°$. Bottom: The simulated axial ratio and return loss of the first loop against various PL angles, with a fixed PL length at 22 mm**

A feeding layer is placed between the radiating layer and a circular aluminium ground plane (45cm **in** diameter). There are three copper arcs in this layer. Each arc has the same curvature as the loop placed above and is placed directly under the loop without touching it. **The lengths and heights of these arcs will affect the antenna's impedance and thus, a parameter sweep is performed in FEKO to optimize both parameters so that a matched impedance of 50Ω can be achieved for each port [3].**

The detailed design procedures of the antenna have been given in [3], here a list of final parameters is shown in Table II.

B. Beam-Scanning Configurations

Using calculations in [8] and [10], it is shown that when the three ports on the antenna are fed with signals of the same amplitude and phase, a tilted beam is formed at $(\theta, \varphi) = (30°, 90°)$. To steer the beam in the azimuth plane by $\Delta\varphi$ degree, the input phase of the middle loop is kept constant, whereas the phase fed to the inner loop and the outer loop is shifted by $+\Delta\varphi$ and $-\Delta\varphi$ respectively.

TABLE II
ANTENNA PARAMETERS, WHERE λ IS 34.6 CM AT 866 MHZ [3]

	First Ring	Second Ring	Third Ring
Perimeter	0.988λ	1.984λ	2.984λ
PL Angle	$45°$	$22.5°$	$-45°$
PL Length	0.058λ	0.065λ	0.061λ
Feed line Length	0.23λ	0.23λ	0.24λ
Feed line Height	0.022λ	0.017λ	0.018λ

To steer the beam in the zenith plane, the total input power is maintained while the amplitude ratio fed to three rings is changed. When an amplitude ratio of 9:1 (inner to middle and outer) is applied, the tilting angle is $0°$. Whereas a $40°$ tilting angle is achieved by using an amplitude ratio of 0:10.

Thus, the antenna's beam can be seamlessly steered from $\theta = 0°$ to $\theta = 40°$ and $\varphi = 0°$ to $\varphi = 360°$ by manipulating the relative phase and amplitude fed to the three loops. **Simulated results are shown in Figures 9 and 10.** It can be seen that the antenna's gain is relatively stable during beam-steering, with the maxima of 10.9 dB at $\theta = 30°$ and the minima of 9.24 dB appearing at $\theta = 40°$.

The antenna's AR minima follows its gain maxima. In the full-wave simulations, it is revealed that when the antenna's beam is tilted at $\theta = 40°$, its 3 dB AR beamwidth is $68°$. Since the antenna's beam is steerable between $\pm 40°$ in θ, an equivalent 3 dB AR beamwidth of $136°$ could be achieved in every φ cut.

III. Antenna Measurement

The proposed antenna is manufactured (as in Fig. 6) and characterised using an MVG StarLab® antenna chamber [2]. A custom PCB board with integrated attenuators and phase shifters is used to vary the phase and amplitude fed to the loops [3]. The measured results are compared with simulation and are shown in Fig. 8 to Fig. 11 [3].

As can be seen the simulation results match well with the measurements. In Fig. 9, it is proven that the antenna can beam-scan from $\theta = 0°$ to $\theta = 40°$ and $\varphi = 0°$ to $\varphi = 360°$. In Fig. 11, it is shown that the antenna's AR minima follows its gain maxima, and a 3 dB AR beamwidth of around $136°$ ($\pm 68°$) is achieved.

The proposed antenna is compared with a commercial 2×2 phased array antenna [3] **of similar size along the diagonal** by measuring both antennas in an MVG StarLab antenna chamber. A summary of their key parameters is shown in Table III. The proposed antenna has a higher gain (around 10.5 dBiC) than the phased array antenna (around 6 dBiC). Its gain is also more stable (**1.1 dBic variation**) during beam-steering than the commercial antenna (**2.5 dBic variation**). In terms of the 3 dB AR beamwidth, the proposed antenna also shows a wider ($136°$) beamwidth than the patch ($45°$). Moreover, it needs no matching network and requires only 2 phase shifters instead of 3 to operate.

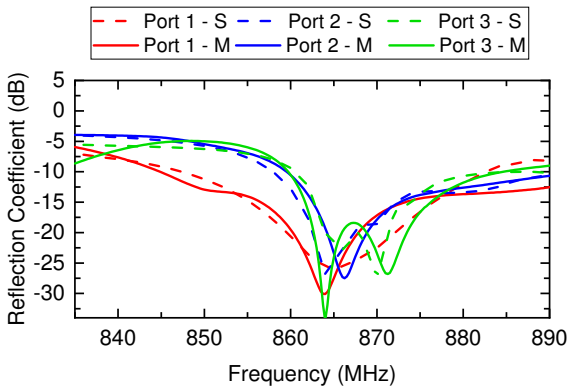

Fig. 8. Simulated and measured return loss of the proposed antenna [3] (M - Measured, S - Simulated). **It is clear from this graph that a -10 dB return loss bandwidth from 860 MHz to 880 MHz is achievable on all three ports of the antenna**

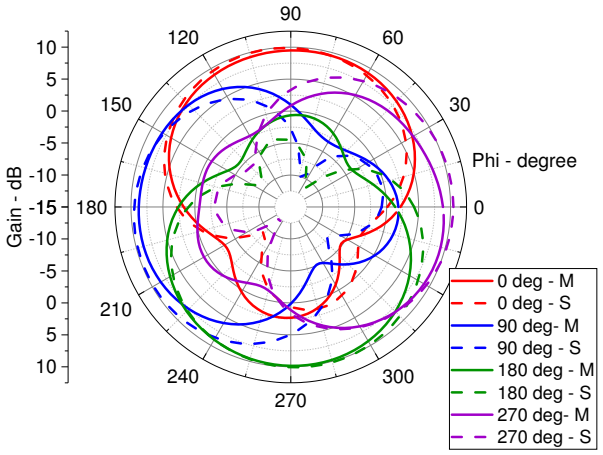

Fig. 9. Simulated and measured total gain of the proposed antennad against φ at $\theta = 30°$ cut. The phase difference between the inner loop and the outer loop varies between $0°$ and $270°$. **Suffix M represent measured results; S represents simulations [3]**

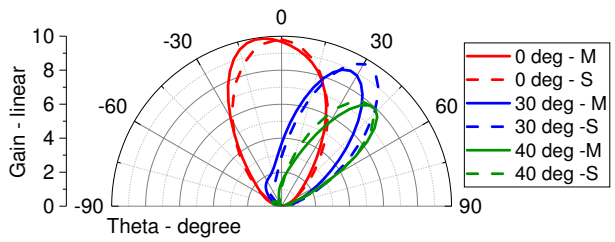

Fig. 10. Simulated and measured total gain of the proposed antenna against θ at $\varphi = 90°$ cut, with **different peak locations due to** different values of the voltage ratio. **Suffix M represent measured results; S represents simulations [3]**

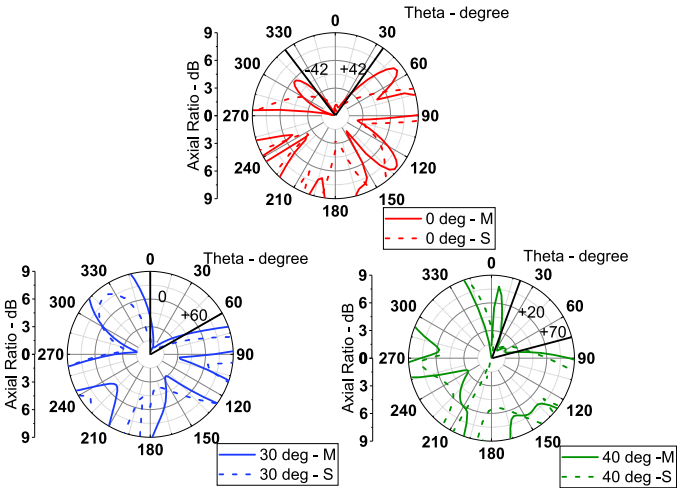

Fig. 11. Simulated and measured axial ratio of the proposed antenna against θ at $\varphi = 90°$ cut, with the peak gain direction at $\theta = 0°, 30°$ and $40°$ respectively. **Suffix M represent measured results; S represents simulations [3]**

TABLE III
A COMPARISON OF THE PROPOSED ANTENNA WITH A COMMERCIAL ANTENNA [3]

	A commercial antenna	The proposed antenna
Size	30cm×30cm	45cm (diameter)
Gain	6 dBic	10.5 dBic
3 dB AR beamwidth	45° (maximum)	136°
Needs Matching Network	Yes	No
Number of Phase Shifters	3	2

IV. Tag Reading Experiments

A. System Configuration

To further verify the read rate improvements of the proposed antenna arising from its 2D beam-scanning ability and improved AR performance, a series of tag reading experiments are conducted.

In these experiments, a custom development board based on Impinj Indy R2000 evaluation module (EVM) [12] is used. The reader architecture in the downlink direction is shown in Fig. 12. The output from the R2000 EVM is **connected to Wilkinson power dividers to create 8 switchable transmit/receive ports**, each followed by an amplifier (qorvo RF3827 [13]), a 180° phase shifter(Mini-Circuits JSPHS-1000 [14]) and a digital attenuator (RFSA2023 [15]) with a 30 dB attenuation range. During these experiments, 3 ports are set to the transmitting mode: one port (port B) is directly connected to the middle ring as the phase reference. To achieve a full 360° phase range, an additional switched 180° phase shift is introduced by feeding the corresponding RF signal through a 180° hybrid phase splitter (Mini-Circuits ZFSCJ-2-4-S+ [16]) and an RF switch (Mini-Circuits ZMSW-1211 [17]). Finally, before the RF signal is fed to the antenna, a WAVELEX WPA0409N power amplifier [18] with a 11 dB gain is used to compensate the loss in the system. Ports D and E are used as receivers while the remaining 3 ports are unused.

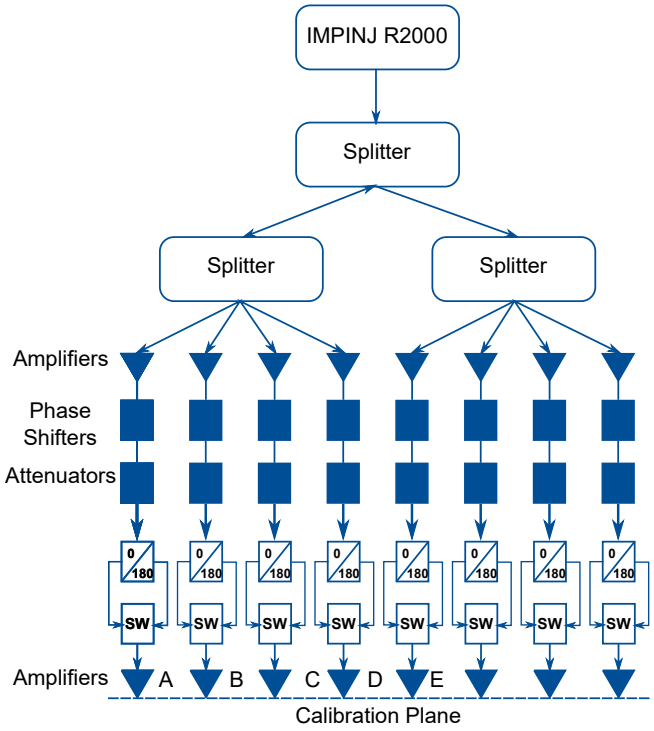

Fig. 12. Architecture of the custom development board based on Indy R2000 [12]. Components on each channel are an amplifier (qorvo RF3827 [13]), a 180° phase shifter(Mini-Circuits JSPHS-1000 [14]) and a digital attenuator (RFSA2023 [15]) respectively

B. Port Calibration

Before the experiments are conducted, the whole system is calibrated to the reference plane as shown in Fig. 12 in terms of phase and amplitude.

1) Phase Calibration: The phase calibration is performed using the system together with a Keysight DSO-S 404A realtime oscilloscope. During the calibration process, port B is connected to channel 1 of the oscilloscope and is used as the phase reference, whereas ports A and C are connected to channel 2 and channel 3 respectively. In each calibration, the phase register of the port being calibrated is changed from 0 to 255 (0x00 to 0xFF) in a step of 1, and in each step the phase difference of the port to port B (the reference port) is queried for 16 times, and the average value is recorded. The result of the phase calibration is shown in Fig. 13.

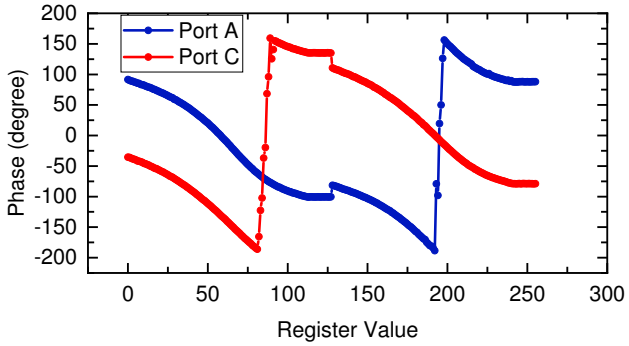

Fig. 13. Phase calibration result of port A and C

It can be seen in Fig. 13 that a phase discontinuity occurs when the phase register value is 128, which is the point when the front end switches introduce an additional 180 degree shift via the hybrid splitters. It is also clear that both ports can perform a 360° phase shift.

A look-up table is generated from the calibration so that an arbitrary phase can be obtained as required, eliminating the non-linearity seen in Fig. 13.

2) Power Calibration: Similar to the phase calibration, the output power of each port is calibrated using an Anritsu MS2690A signal analyser. The recorded characteristic of the 3 transmit ports is shown in Fig. 14. **Again a look up table is used to correct for the offsets and non-linearity.**

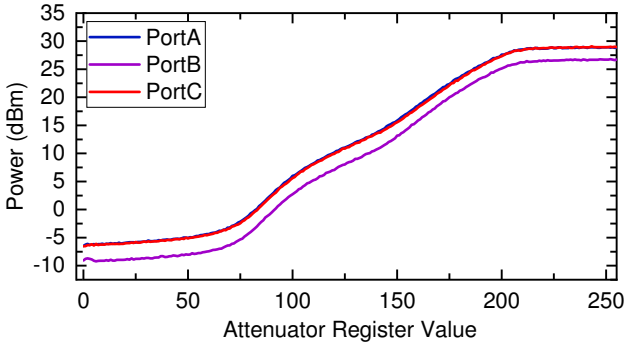

Fig. 14. Power calibration result of port A, B and C

C. Test Environment

In the following experiments, the reader antenna is placed on the ceiling (3 metres high) in the centre of a $3m \times 5m$ room, facing downwards. Two CP receiving antennas (MT-242027/NRH/K [19]) are placed in the corners of the room, facing 45° downwards and are connected to two receiving ports (port D and E of the development board) **since the development board is not able to operate in a monostatic configuration**. 300 RFID tags (AVERY DENNISON AD-236u7 [20]) are placed in random locations and orientations in the room, as shown in Fig. 15.

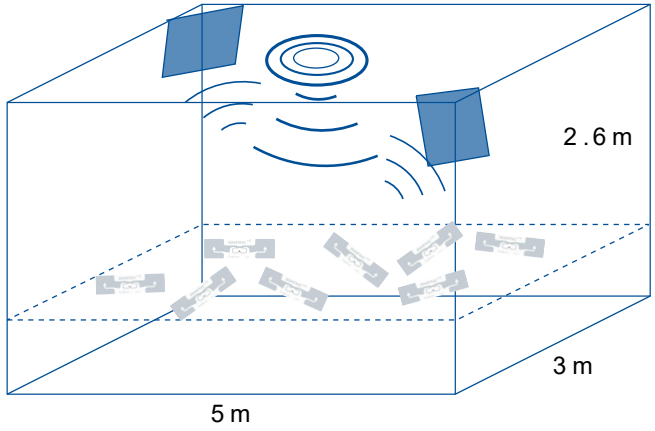

Fig. 15. The test environment

The experiment is divided into two stages: (i) to verify the improvement of 2D beam-scanning over a static beam and a 1D beam-scanning; and (ii) to verify the improvement resulting from the better AR performance.

In all these experiments, the reader is configured to output 26 dBm power at the reference plane, so that with the antenna's 10 dB gain and the losses of the coaxial cables, the effective isotropic radiated power (EIRP) is less than 35 dBm, compliant with regulations by the European Telecommunications Standards (ETSI). The total inventory time is set to be 120 seconds, and the curve of remaining undetected tags versus time is drawn, as an indication of the overall performance.

1) Static Beam and 1D/2D Beam-scanning: In this step of the experiment, the antenna is configured into three status:

- **Static beam:** the antenna is configured to generate a static beam, with its 9 dB maxima pointed at $(\theta, \varphi) = (0°, 0°)$.
- **1D beam-scanning:** the antenna is configured to scan its beam by changing the phase inputs, so that its maxima is pointed at $(\theta, \varphi) = (30°, \Delta\varphi)$, where $\Delta\varphi$ is from 0° to 360°.
- **2D beam-scanning:** by varying the input power and phase, the antenna's beam maxima is pointed at $(\theta, \varphi) = (\Delta\theta, \Delta\varphi)$, where $\Delta\theta$ is from 0° to 40° and $\Delta\varphi$ is from 0° to 360°.

The results of this step are shown in Fig. 16. The number of tags remaining undetected after 120 seconds dropped from 105 with the static beam configuration to 12 with 1D beam-scanning, and to 0 with the 2D beam-scanning. **The reduction in the number if missing tags shows the superiority of using 2D beam-scanning over 1D.**

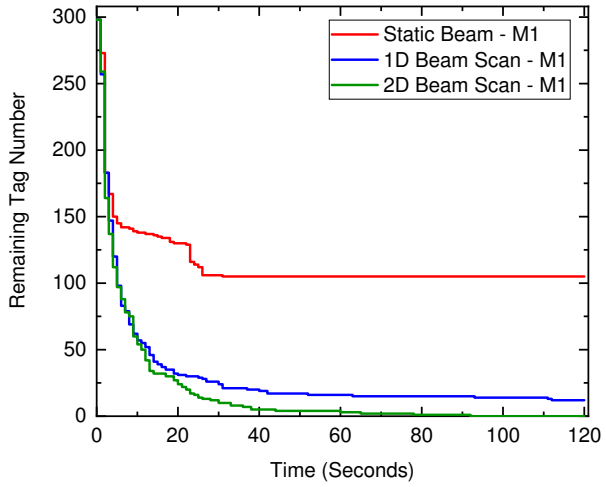

Fig. 16. The number of remaining tags versus time, comparing static beam and 1D/2D beam-scanning.

2) AR Performance: In practical RFID applications, tags are almost always linearly polarised and randomly oriented. Thus, it is often assumed that an improved AR performance would lead to a better tag-reading performance, as CP antennas can minimise the polarisation mismatch between the tags and the reader antennas. However, since it is hard to change AR alone without significantly changing other antenna parameters, it is difficult to quantify how much improvement comes from differences in AR rather than from differences in **e.g. gain** or beamwidth, when comparing two antennas.

The proposed antenna has a unique advantage in solving this problem; our paper [9] **has verified** through simulations and experiments that the **proposed** antenna's AR performance depends on the length and position of the perturbation lines, whereas its gain and beamwidth are affected by loop perimeters and their distances from the ground plane [8]. Using this insight, a new antenna with a degraded AR performance is constructed by trimming the PL of three rings by 2.5 mm. The parameters of the degraded-AR antenna, including its return loss, gain pattern and AR performance are shown in Fig. 17 to Fig. 20.

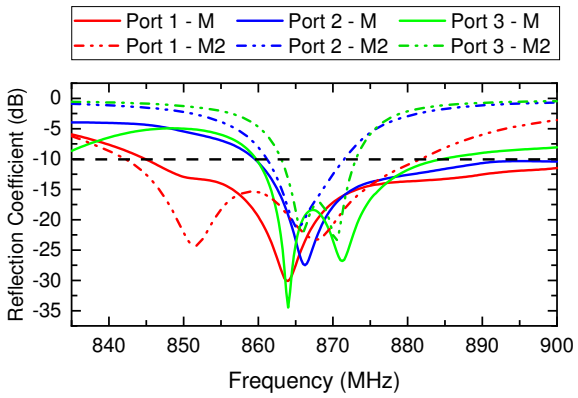

Fig. 17. The measured reflection coefficient of the original antenna (M) and the new antenna with degraded AR performance (M2) [9]

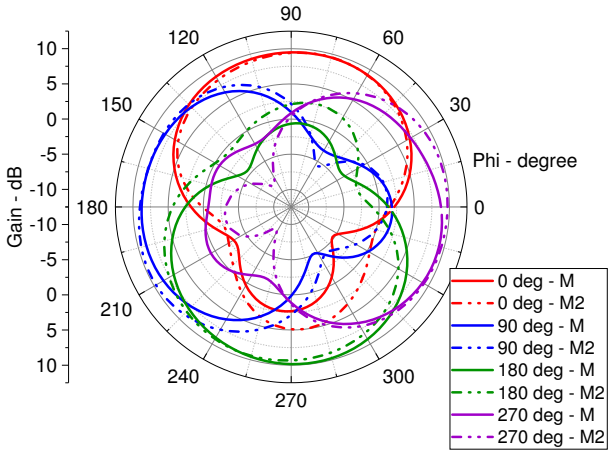

Fig. 18. The measured gain pattern against φ at $\theta = 30°$ cut of the original antenna (M) and the new antenna with degraded AR performance (M2)

From Fig. 17, the return loss of the antenna is degraded, but still below -10 dB in the desired frequency range. Fig. 18 and Fig. 19 reveal that the beam-width of the antenna is virtually the same as the original design, with a slightly degraded side-lobe performance. The peak gain is reduced by 0.7 dB but can be compensated by increasing the input power.

Thus, a degraded antenna is obtained with the same gain and beamwidth, but a degraded AR performance (**Fig. 20**). The tag

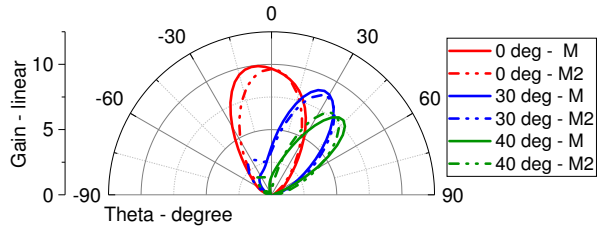

Fig. 19. The measured gain pattern against θ at $\varphi = 90°$ cut of the original antenna (M) and the new antenna with degraded AR performance (M2)

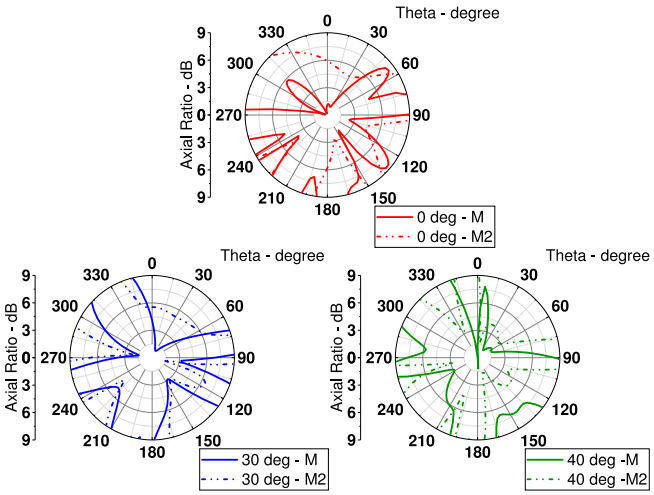

Fig. 20. The measured AR performance of the original antenna (M) and the new antenna with degraded AR performance (M2)

reading experiments described in section IV are repeated and the results are shown in Fig. 21.

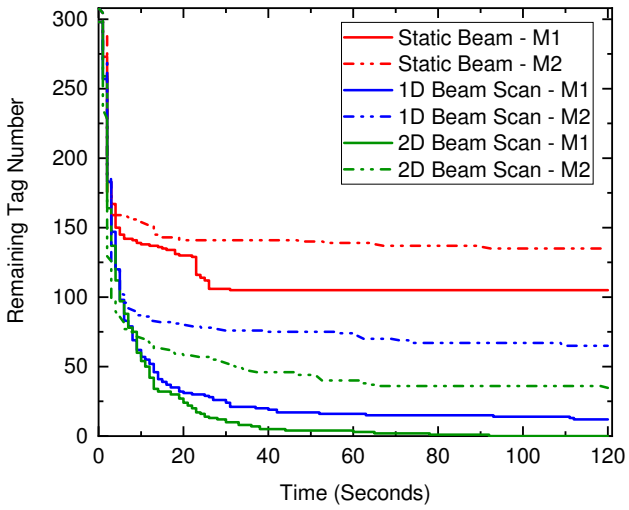

Fig. 21. The number of remaining tags versus time, comparing static beam and 1D/2D beam-scanning of the original antenna with optimised AR (M1) and the new antenna with degraded AR (M2)

It can be seen that tag-reading performance is greatly affected by the AR performance. Specifically, the number of remaining tags rises from 105 to 135 in a static beam configuration, from 12 to 65 in a 1D beamscanning configuration, **and from** 0 to 34 in a 2D beamscanning configuration **when the AR is degraded**. This verifies that the antenna's improved AR performance does lead to a superior tag-reading performance. Moreover, as per regulations by ETSI [21], EIRP is relative to the power measured in the maximum linear polarisation, thus a **larger** AR would reduce the maximum allowed conducted power of the antenna, potentially resulting in even greater degradation of read performance with axial ratio.

V. Conclusion

A novel antenna with 2D beam-scanning ability, wide axial ratio beamwidth and simple configuration is designed, simulated, measured and tested. It is compared with both beam-scanning antennas in literature and a commercial phased array antenna, and is shown to possess key advantages in terms of design complexity, beam-scanning abilities and AR performance. The antenna features an ultra-wide 3 dB AR beamwidth of 136°, 2D beam-scanning from 0° to 360° in the azimuth plane and 0° to 40° in the elevation plane. The antenna has a unique property of changing its AR without significantly affecting other properties. Utilizing this property, it **has been experimentally shown** that the antenna's 2D beamscanning ability and its superior AR performance lead to significant improvements in tag reading.

References

[1] D. Dobkin, *The RF in RFID: UHF RFID in practice*. Newnes, 2012.

[2] MVG. (2019) StarLab. Accessed on: May 5, 2019. [Online]. Available: https://www.mvg-world.com/en/products/field_product_family/antenna-measurement-2/starlab

[3] R. Chen, S. Yang, A. M. Ndifson, I. H. White, R. V. Penty, and M. Crisp, "Beam scanning UHF RFID reader antenna with high gain and wide axial ratio beamwidth," in *2019 IEEE International Conference on RFID Technology and Applications (RFID-TA)*, Sep. 2019, pp. 374–379.

[4] C. Liu, S. Xiao, Y.-X. Guo, Y.-Y. Bai, and B.-Z. Wang, "Broadband circularly polarized beam-steering antenna array," *IEEE Transactions on Antennas and Propagation*, vol. 61, no. 3, pp. 1475–1479, 2012.

[5] S.-L. Chen, P.-Y. Qin, W. Lin, and Y. J. Guo, "Pattern-reconfigurable antenna with five switchable beams in elevation plane," *IEEE Antennas and Wireless Propagation Letters*, vol. 17, no. 3, pp. 454–457, 2018.

[6] K. Hirose, S. Okazaki, and H. Nakano, "Double-loop antennas for a circularly polarized tilted beam," *Electronics and Communications in Japan (Part I: Communications)*, vol. 86, no. 12, pp. 12–20. [Online]. Available: https://onlinelibrary.wiley.com/doi/abs/10.1002/ecja.10132

[7] W. Hu, G. Wen, D. Inserra, Y. Huang, J. Li, and Z. D. Chen, "A circularly polarized antenna array with gain enhancement for long-range UHF RFID systems," *Electronics*, vol. 8, no. 4, p. 400, 2019.

[8] C. A. Balanis, *Antenna theory: analysis and design*. John wiley & sons, 2016.

[9] R. Chen, S. Yang, A. M. Ndifson, I. H. White, R. V. Penty, and M. Crisp, "A UHF RFID reader antenna with tunable axial ratio and fixed beamwidth," in *14th European Conference on Antennas and Propagation (EuCAP) 2020*. IEEE, 2020, (To be published).

[10] T. Nakamura and S. Yokokawa, "Loop antenna with a branch wire for circular polarization," *Electronics and Communications in Japan (Part I: Communications)*, vol. 70, no. 11, pp. 110–117, 1987.

[11] H. Nakano, "A numerical approach to line antennas printed on dielectric materials," *Computer physics communications*, vol. 68, no. 1-3, pp. 441–450, 1991.

[12] IMPINJ. (2019, oct) Indy r2000 rain rfid reader chip. Accessed on: Oct 5, 2019. [Online]. Available: https://www.impinj.com/platform/connectivity/indy-r2000/

[13] Qorvo. (2019, oct) Rf3827 5 - 1500 mhz linear general purpose amplifier. Accessed on: Oct 5, 2019. [Online]. Available: https://www.qorvo.com/products/p/RF3827

[14] Mini-Circuits. (2019, oct) Jsphs-1000+ phase shf / surf mt / rohs. Accessed on: Oct 5, 2019. [Online]. Available: https://www.minicircuits.com/WebStore/dashboard.html?model=JSPHS-1000%2B

[15] Qorvo. (2019, oct) Rfsa2023 50 - 6000 mhz, 3.3 v voltage controlled attenuator. Accessed on: Oct 5, 2019. [Online]. Available: https://www.qorvo.com/products/p/RFSA2023

[16] Mini-Circuits. (2019, oct) Zfscj-2-4-s+ connector 180 hybrid, 50 - 1000 mhz. Accessed on: Oct 5, 2019. [Online]. Available: https://www.minicircuits.com/WebStore/dashboard.html?model=ZFSCJ-2-4-S%2B

[17] Mini-Circuits. (2019, oct) Zmsw-1211 reflective spdt. Accessed on: Oct 5, 2019. [Online]. Available: https://www.minicircuits.com/WebStore/dashboard.html?model=ZMSW-1211

[18] Wavelex. (2019, oct) Amplifiers: 1 to 1400 mhz pa, n-connectorized. Accessed on: Oct 5, 2019. [Online]. Available: http://www.wavelex.com/products/?category=60

[19] M. W. E. LTD. (2019, oct) Mt-242027/nrh/k 865 - 870 mhz, 8.5dbic rhcp reader antenna. Accessed on: Oct 5, 2019. [Online]. Available: https://www.mtiwe.com/?CategoryID=278\&ArticleID=56

[20] A. DENNISON. (2018, oct) Uhf rfid inlaysad-236u7. Accessed on: Oct 5, 2019. [Online]. Available: https://rfid.averydennison.com/content/dam/averydennison/rfid/Global/Documents/datasheets/AD-236u7-Datasheet-v3.pdf

[21] E. T. S. Institute. (2018, feb) Draft etsi en 302 208 v3.2.0 (2018-02). [Online]. Available: https://www.etsi.org/deliver/etsi_en/302200_302299/302208/03.02.00_20/en_302208v030200a.pdf,note=